

Continuous near-field electrospinning for large area deposition of orderly nanofiber patterns

Chieh Chang,^{a)} Kevin Limkrailassiri, and Liwei Lin

Berkeley Sensor and Actuator Center, Department of Mechanical Engineering, University of California, Berkeley, California 94720, USA

(Received 30 June 2008; accepted 4 August 2008; published online 24 September 2008)

A continuous near-field electrospinning (NFES) process has been developed to deposit solid nanofibers with orderly patterns over large areas. Before the onset of electrospinning, a bias voltage is applied to a semispherical shaped polymer droplet outside of a syringe needle, and a probe tip mechanically draws a single fiber from the droplet to initiate continuous NFES. Contrary to the conventional electrospinning process, we show that decreasing electrical field in continuous NFES results in smaller linewidth deposition, and nanofibers can be assembled into controlled complex patterns such as circular shapes and grid arrays on large and flat areas. © 2008 American Institute of Physics. [DOI: 10.1063/1.2975834]

Conventional electrospinning processes producing randomly deposited nanofibers have been used in various applications including filtration,¹ texturing,² composite reinforcement,^{3,4} and tissue scaffolds.⁵ The disorderly fashion of such deposited nanofibers, however, has limited its full potential. For example, well-controlled architectures, rather than random configurations, could give rise to improvements in the aforementioned examples as well as other applications. Several groups in recent years have been developing orderly electrospinning processes using dynamic mechanical devices to improve the alignment and placement of electrospun nanofibers, including the use of a wheel-like reel, which has been shown to position and align individual polymer nanofibers into parallel arrays.^{6–8} However, highly aligned nanofibers in a large and flat area are difficult to achieve using this method. Manipulation of electrical field has been exploited as well, including the use of an electrostatic lens element and collection target of opposite polarity, which has been implemented to dampen bending instability and control deposition,⁹ aligned yarns of nylon-6 nanofibers, which have been collected by rapidly oscillating a grounded frame within the jet,¹⁰ the use of a metal frame as the collector, which can also generate parallel arrays of polyamide nanofibers,¹¹ and the use of electrostatic forces guiding fibers across voids in the collector.^{12,13} The combination of dynamic mechanical devices and manipulation of electrical field can fabricate better aligned nanofiber patterns as parallel arrays and grids.^{14,15} However, these methods do not have good control on the pitch width and cannot make complex patterns such as circles. Buckling phenomena have also been studied in which electrically charged jets impinge onto collectors moving laterally at a constant velocity to produce buckling patterns with limited controllability.¹⁶ On the other hand, electrospinning using short needle-to-collector distance, including scanning tip electrospinning¹⁷ and near-field electrospinning¹⁸ (NFES), has shown easier and more predictable location control for the deposition of nanofibers. However, the polymer droplet approach in these processes limits the total length of nanofiber deposition, and fiber thickness is inevitably nonuniform because the polymer droplet is consumed during the process. Herein, we propose

and demonstrate the principle and methodology of continuous NFES, which benefits from the continuity of conventional electrospinning and the superior location control of NFES to produce orderly nanofiber patterns over large areas.

In the conventional electrospinning process, the applied electrical field generates sufficient electrostatic forces to deform the polymer meniscus into a conical shape called a Taylor cone.¹⁹ A critical electrical field at which electrostatic forces overcome the surface tension forces is required to induce a polymer jet from the tip of Taylor cone.¹⁹ Typically the critical electrical field of conventional electrospinning process is on the order of 10^5 V/m.²⁰ In our experimental demonstration, 7 wt % polyethylene oxide (PEO) ($M_v = 300\,000$) aqueous solution is used under room temperature and 1 atm of pressure. The needle-to-collector distance is fixed at 500 μm and a syringe needle with 200 μm outer diameter and 100 μm inner diameter is utilized as the spinneret to continuously supply polymer solution. Figure 1(a) shows that the applied voltage on the syringe needle reaches a critical value of 1.5 kV for jet initiation and the cone has a semivertical angle of around 49° . The corresponding critical electrical field (3×10^6 V/m) is one order of magnitude larger than that of conventional electrospinning because the surface tension of the droplet increases as syringe needle diameter decreases. The polymer jet below the tip of the cone is about 25 μm in diameter, similar to that of the conventional electrospinning process in which the needle-to-collector distance is about 5–50 cm. However, since the needle-to-collector distance is only 500 μm in the near-field setup, the solvent in the polymer jet does not have enough time to fully evaporate. As a result, as-spun fibers are 3–6 μm in diameter and remain in liquid form shortly after deposition as shown in Fig. 1(b). Oftentimes, consequent fibers will merge with those that have just deposited onto the collector.

In order to have electrospun nanofibers with diameter in the sub-100 nm range, the applied electrical field for conventional electrospinning can be increased to cause greater stretching of the polymer solution. However, the controllability of nanofiber deposition is severely affected by bending instability.²¹ The key strategy for producing sub-100 nm nanofibers via NFES, on the other hand, is to reduce the size of the polymer jet emerging from the cone by reducing the

^{a)}Electronic mail: chieh@berkeley.edu.

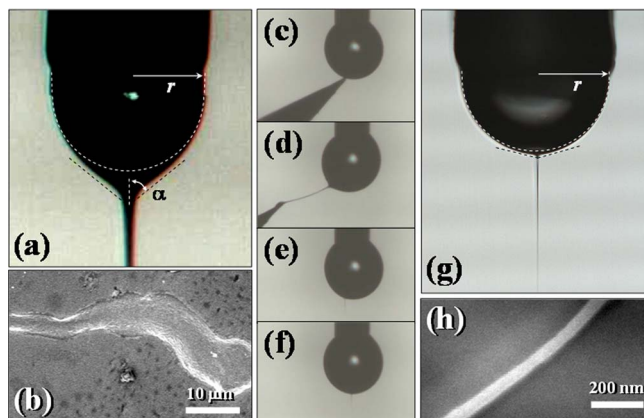


FIG. 1. (Color online) (a) The syringe needle ($r=100\ \mu\text{m}$), droplet, and cone ($\alpha=49^\circ$) of conventional electrospinning in near-field setup where applied voltage is 1.5 kV and needle-to-collector distance is $500\ \mu\text{m}$. The white dashed curve represents the fluid surface just before jet initiation and the cone part is the fluid surface right at jet initiation. (b) The as-spun fibers from (a). (c) A tungsten probe tip poking inside the polymer meniscus. (d) Mechanical drawing of a fiber from polymer droplet. (e) The electrospinning process is initiated. (f) The polymer jet automatically moves downward due to the applied electrical field. (g) The syringe needle ($r=100\ \mu\text{m}$), droplet, and cone ($\alpha=75^\circ$) of continuous NFES. The process is initiated with the aid of a probe tip at a voltage of 600 V while the needle-to-collector distance is $500\ \mu\text{m}$. (h) The as-spun fibers from (g).

applied electrical field below the critical value. Theoretically, this can be accomplished by simultaneously reducing the applied voltage and polymer solution supply rate after the onset of electrospinning is achieved [Fig. 1(a)]. Practically, this is very difficult to control as a high supply rate would result in excess polymer plummeting to the collector, disrupting the delicate electrospinning process, while a low supply rate would cause the pendant droplet to shrink quickly and terminate the electrospinning process. To circumvent the limitations of these approaches, we have developed a simple and reliable technique to achieve continuous NFES by means of an initial mechanical drawing process that aids electrical force in overcoming surface tension to initiate the ejection of a polymer jet. This process starts by applying a subcritical voltage to deform the polymer meniscus without inducing electrospinning. Mechanical drawing is applied by using a tungsten probe with $1\ \mu\text{m}$ tip diameter to poke inside the meniscus. The probe is then rapidly pulled away from the polymer droplet to activate the continuous electrospinning process as illustrated in Figs. 1(c)–1(e). The initial location of the probe tip is not crucial since the polymer jet will automatically move downward and align to the applied electrical field as shown in Figs. 1(e) and 1(f). Instead of mechanical drawing, the subcritical voltage is the key control parameter in deciding the size of deposited nanofibers as evidenced in Fig. 1(d) where the fiber jet is relatively thick during the mechanical drawing process while Figs. 1(e) and 1(f) show thinner fiber jet after the mechanical probe is removed. In this case as shown in Fig. 1(g), the applied voltage is 600 V, corresponding to an electrical field of $1.2 \times 10^6\ \text{V/m}$, and the polymer jet diameter immediately outside of the cone is about $3\ \mu\text{m}$, and the deposited nanofibers on the collector have diameters of about $50\ \text{nm}$ as shown in Fig. 1(h). The semivertical angle of the cone is 75° . A polymer feed rate of about $0.1\ \mu\text{L/h}$ can maintain the droplet shape for continuous and uniform deposition of nanofibers. With the aid of this initial mechanical drawing process, con-

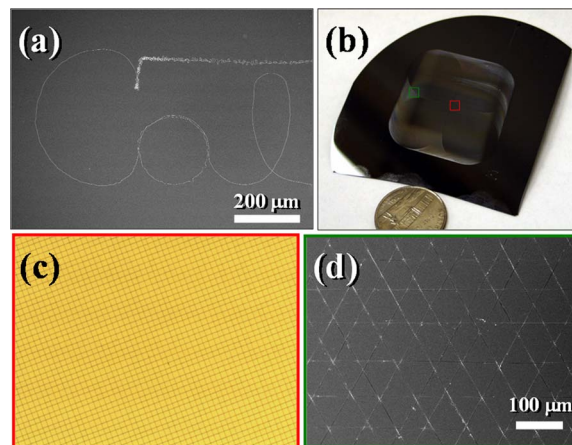


FIG. 2. (Color online) (a) The three-character Cal is drawn on a silicon chip by a programmable x - y stage. (b) A single nanofiber deposited on a silicon chip in a designed trajectory covers a $4 \times 4\ \text{cm}^2$ area in 15 min via continuous NFES. The background is a US quarter. (c) A grid pattern with controlled $50\ \mu\text{m}$ spacing from an area highlighted by the red box in (b). (d) A triangular pattern from an area highlighted by the green box in (b).

tinuous supply of polymer solution is maintained for NFES while the size of polymer jet emerging from the cone is drastically reduced to achieve sub-100 nm deposition of nanofibers. Moreover, this approach avoids the cumbersome issue of consistently extruding a polymer droplet of the same size through a syringe needle of small diameter.

To demonstrate the controllability and continuity of this process, variety of orderly patterns are deposited onto silicon collectors using a programmable x - y stage (Newport, Inc.). Experimentally, the syringe needle is fixed while the stage translates at a speed of $120\ \text{mm/s}$. Figure 2(a) shows the smooth writing of “Cal” in an area of $1 \times 0.5\ \text{mm}^2$ where the diameter of the fiber is $150\ \text{nm}$. The smoothness of the pattern was achieved by setting the translational speed of the stage as close as possible to the deposition rate. A slow translational speed would cause the nanofiber to form spiraling patterns as shown in the region preceding the script “C” in Fig. 2(a), while a high translational speed would not afford the nanofiber enough time to anchor itself at all points on the intended pattern. A circular design, for instance, would appear as a polygonal nanofiber pattern. Additionally, the size of the pattern in Fig. 2(a) does not represent the smallest design that can be drawn using continuous NFES. Since the speed of the x - y stage must match the electrospinning deposition rate for smoothness, this criteria must be met regardless of the intricacy of the pattern; however, smaller arc trajectories demand extremely large radial acceleration, and the extent to which this acceleration can be executed depends on the capabilities of the x - y stage. Figure 2(b) illustrates experimental results of the continuous NFES of a single nanofiber deposited on a silicon chip in a designed trajectory over a $4 \times 4\ \text{cm}^2$ large area. The process can continue running as long as polymer solution is supplied from the syringe needle. In this case, the deposition period is 15 min for a total length of $108\ \text{m}$ and the nanofiber has a diameter of $709 \pm 131\ \text{nm}$. The diameter and standard deviation are calculated based on 100 data points measured directly from scanning electron microscopy (SEM). The optical image in Fig. 2(c) shows that the nanofiber is deposited on the silicon chip with a fiber pitch of $49.88 \pm 3.98\ \mu\text{m}$ (from 50 data points) while the designed trajectory has a fiber pitch of $50\ \mu\text{m}$. We believe

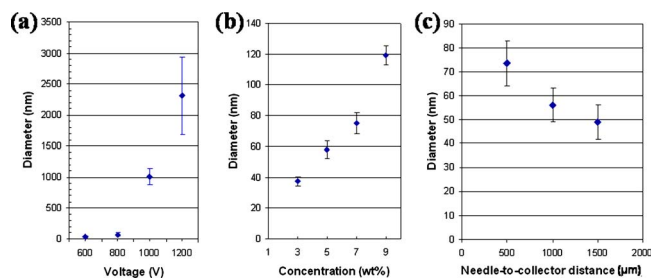


FIG. 3. (Color online) Plots showing the dependence of nanofiber diameters on various processing parameters. (a) Applied voltage. Other parameters are maintained as the following: PEO concentration (7 wt %) and needle-to-collector distance (500 μm). (b) Polymer concentration. Other parameters are maintained as the following: applied voltage (500 V) and needle-to-collector distance (1000 μm). (c) Needle-to-collector distance. Other parameters are maintained as the following: PEO concentration (7 wt %) and applied voltage (800 V). All experiments are under room temperature and 1 atm pressure.

that this uneven spacing is mainly due to the oscillation of the cone on the polymer droplet, which is caused by the interference of the fiber charges with the electrical field, mechanical buckling during impact between polymer jet and collector,¹⁶ and external perturbations.²¹ Further investigation is required in order to minimize such errors on nanofiber deposition. A triangular pattern is also deposited using the same process, as shown in Fig. 2(d).

Similar to the conventional electrospinning process, the diameter of nanofibers could be adjusted by controlling various operating parameters. The following characterization of fiber diameters and standard deviation are calculated based on 50 data points measured directly from SEM in each experiment. When the PEO concentration is 7 wt % and the needle-to-collector distance is fixed at 500 μm , the average fiber diameter can be varied in the range of 38 ± 4 to 2314 ± 622 nm under different applied voltages as shown in Fig. 3(a). The proportional relationship between the fiber diameter and applied voltage confirms the previous observation that the cone size and polymer jet both increase with applied electrical field. Therefore, higher voltage results in thicker fibers in continuous NFES, which is contrary to the trends observed in conventional electrospinning.^{22–24} In the conventional electrospinning process, higher bias voltages imply stronger Coulombic repulsion force in the polymer jet to further stretch the nanofibers during the whipping process. In the continuous NFES process, this effect is diminished due to short needle-to-collector distance such that the initial polymer jet diameter dominates the final nanofiber diameter rather than bending instability.

The polymer concentration also affects the morphology of the electrospun nanofibers. If the PEO solution concentration is lower than approximately 3 wt %, the continuous NFES process cannot be activated due to its insufficient viscoelasticity. At such low polymer concentrations, the elongational viscosity is insufficient to suppress capillary breakup. When the polymer concentration is increased nanofibers are obtained due to an increase in viscosity. As shown in Fig. 3(b), the average fiber diameter can range from 37 ± 3 to 119 ± 6 nm by increasing the polymer concentration when the needle-to-collector distance is fixed at 1000 μm under a bias voltage of 500 V. The needle-to-collector distance is another key factor that affects the diameters of deposited nanofibers. As shown in Fig. 3(c), larger needle-to-collector

distance results in thinner fibers due to a longer period of stretching as polymer jets travel toward the collector. The average fiber diameter ranges from 49 ± 7 to 74 ± 9 nm when the applied voltage is 800 V and the concentration of PEO solution is 7 wt %.

The concept and demonstration of continuous NFES make possible applications that were difficult to achieve by conventional electrospinning. We believe that the ability to deposit polymeric materials at precise locations with specific patterns can open up opportunities for cost-effective heterogeneous integration of a variety of materials. There are many areas to be explored with the utilization of continuous NFES. For example, continuous NFES has the potential to create highly ordered and customized patterns through automated processes to create scaffolds that are highly representative of extracellular matrix. Using continuous NFES, nanofiber arrays and grids can be manufactured over large areas and controlled with precision on the same length scales at the cellular level, enabling the development of cell culture substrates that are vastly customizable. Such scaffolds could potentially extend current tissue engineering techniques to develop previously unachievable substrate types and increase the viability of these tissues.

The authors would like to thank UC Berkeley Microfabrication Laboratory for their support, Miss Yuan Gao for assistance with the electrospinning work, and Miss Adrienne Higa for the discussions. This work was supported in part under DARPA MTO MEMS/NEMS S&T program and a NSF under Grant No. EEC-0425914.

- ¹P. Gibson, H. Schreuder-Gibson, and D. Rivin, *Colloids Surf., A* **187-188**, 469 (2001).
- ²K. J. Pawlowski, H. L. Belvin, D. L. Raney, J. Su, J. S. Harrison, and E. J. Siochi, *Polymer* **44**, 1309 (2003).
- ³Y. Dzenis and Y. Wen, *Mater. Res. Soc. Symp. Proc.* **702**, 173 (2002).
- ⁴H. Ye, H. Lam, N. Titchenal, Y. Gogotsi, and F. Ko, *Appl. Phys. Lett.* **85**, 1775 (2004).
- ⁵L.-S. Yeo, J.-E. Oh, L. Jeong, T. S. Lee, S. J. Lee, W. H. Park, and B.-M. Min, *Biomacromolecules* **9**, 1106 (2008).
- ⁶J. A. Matthews, G. E. Wnek, D. G. Simpson, and G. L. Bowlin, *Biomacromolecules* **3**, 232 (2002).
- ⁷P. Katta, M. Alessandro, R. D. Ramsier, and G. G. Chase, *Nano Lett.* **4**, 2215 (2004).
- ⁸L. Wannatong, A. Sirivat, and P. Supaphol, *Polym. Int.* **53**, 1851 (2004).
- ⁹J. M. Deitzel, J. Kleinmeyer, J. K. Hirvonen, and T. N. C. Beck, *Polymer* **42**, 8163 (2001).
- ¹⁰H. Fong, W.-D. Liu, C.-S. Wang, and R. A. Vaia, *Polymer* **43**, 775 (2002).
- ¹¹R. Dersch, T. Liu, A. K. Schaper, A. Greiner, and J. H. Wendorff, *J. Polym. Sci. A* **41**, 545 (2003).
- ¹²D. Li, Y. Wang, and Y. Xia, *Nano Lett.* **3**, 1167 (2003).
- ¹³D. Li, Y. Wang, and Y. Xia, *Adv. Mater. (Weinheim, Ger.)* **16**, 361 (2004).
- ¹⁴A. Theron, E. Zussman, and A. L. Yarin, *Nanotechnology* **12**, 384 (2001).
- ¹⁵E. Zussman, A. Theron, and A. L. Yarin, *Appl. Phys. Lett.* **82**, 973 (2003).
- ¹⁶T. Han, D. H. Reneker, and A. L. Yarin, *Polymer* **48**, 6064 (2007).
- ¹⁷J. Kameoka, R. Orth, Y. Yang, D. Czaplowski, R. Mathers, G. W. Coates, and H. G. Craighead, *Nanotechnology* **14**, 1124 (2003).
- ¹⁸D. Sun, C. Chang, S. Li, and L. Lin, *Nano Lett.* **6**, 839 (2006).
- ¹⁹G. Taylor, *Proc. R. Soc. London* **280**, 383 (1964).
- ²⁰D. H. Reneker and I. Chun, *Nanotechnology* **7**, 216 (1996).
- ²¹D. H. Reneker, A. L. Yarin, H. Fong, and S. Koombhongse, *J. Appl. Phys.* **87**, 4531 (2000).
- ²²J. S. Lee, K. H. Choi, H. Do Ghim, S. S. Kim, D. H. Chun, H. Y. Kim, and W. S. Lyoo, *J. Appl. Polym. Sci.* **93**, 1638 (2004).
- ²³C. J. Buchko, L. C. Chen, Y. Shen, and D. C. Martin, *Polymer* **40**, 7397 (1999).
- ²⁴S. Megelski, J. S. Stephens, D. B. Chase, and J. F. Rabolt, *Macromolecules* **35**, 8456 (2002).